Dual-frequency laser comprising a single fiber ring cavity for self-injection locking of DFB laser diode and Brillouin lasing

VASILY V. SPIRIN,[1] JOSÉ L. BUENO ESCOBEDO,[1] DMITRY A. KOROBKO,[2] PATRICE MÉGRET,[3] AND ANDREI A. FOTIADI[2,3,4,*]

[1]*Scientific Research and Advanced Studies Center of Ensenada (CICESE), Carretera Ensenada-Tijuana No. 3918, Zona Playitas, 22860 Ensenada, B.C., Mexico*
[2]*Ulyanovsk State University, 42 Leo Tolstoy Street, Ulyanovsk, 432970, Russia*
[3]*University of Mons, Electromagnetism and Telecommunication Department, B-7000 Mons, Belgium*
[4]*Ioffe Physical-Technical Institute, RAS, 26 Polytekhnicheskaya Street, St. Petersburg 194021, Russia*
*Andrei.Fotiadi@gmail.com

Abstract: Low-noise lasers are a powerful tool in precision spectroscopy, displacement measurements, and development of advanced optical atomic clocks. While all applications benefit from lower frequency noise and robust design, some of them also require lasing at two frequencies. Here, we introduce a simple dual-frequency laser leveraging a ring fiber cavity exploited both for self-injection locking of a standard semiconductor distributed feedback (DFB) laser and for generation of Stokes light via stimulated Brillouin scattering. In contrast to the previous laser configurations, the system is supplied by a low-bandwidth active optoelectronic feedback. Importantly, continuous operation of two mutually locked frequencies is provided by self-injection locking, while the active feedback loop is used just to support this regime. The fiber configuration reduces the natural Lorentzian linewidth of light emitted by the laser at pump and Stokes frequencies down to 270 Hz and 110 Hz, respectively, and features a stable 300-Hz-width RF spectrum recorded with beating of two laser outputs. Translating the proposed laser design to integrated photonics will dramatically reduce cost and footprint for many laser applications such as ultra-high capacity fiber and data center networks, atomic clocks, and microwave photonics.

1. Introduction

Linewidth narrowing and stabilization of semiconductor laser light generation is of great research interest governed by huge demand of compact cost-effective narrow-band laser sources for many potential applications [1–8]. In 2012 we have demonstrated a simple kHz-linewidth laser just splicing a standard distributed feedback (DFB) laser diode and a few passive telecommunication components [9]. The principle of operation employs the mechanism of self-injection locking that significantly improves DFB laser performance [10–14]. While a typical linewidth of free-running DFB semiconductor lasers ranges from a few to tens MHz, self-injection locking of a DFB laser through an external fiber ring cavity causes a drastic reduction of its laser linewidth down to a few kHz. The main drawback of this technique is its high sensitivity to fluctuations of the configuration parameters and surroundings.

Several approaches have been performed to stabilize the laser operation in the self-injection locking regime [15–18]. Once getting locking to the cavity resonance, the laser starts to generate the cavity resonant frequency. Then any slow change of the ring mode frequency (due to environmental temperature fluctuations, for example) near the stability point causes the same change of the laser frequency [19,12]. However, a more extended drift of the cavity mode frequency (>10 MHz) causes mode-hopping making laser operation temporally unstable. In our

previous experiments, a stable laser operation has been commonly observed for a few seconds. With precise stabilization of the laser diode current and temperature applied in conjugation with a thermal control of a whole fiber configuration the time of a stable laser operation could be extended to tens of minutes [18] and even more [20]. However, these stabilization solutions are technically complicated and rather costly.

An alternative solution has been proposed recently [21]. We have demonstrated stabilization of a semiconductor DFB laser in self-injection locking regime implementing an active optoelectronic feedback controlled by a low-cost USB-DAQ card. In this approach, a narrowing of DFB laser linewidth is still provided by the self-injection-locking mechanism, whereas the active feedback is used to maintain the laser operation in this regime. Therefore, in terms of a feedback circuit bandwidth, complexity, and allocated memory, this method is much less consuming than optoelectronic systems commonly used with fiber lasers [22,23]. The advantage of the proposed configuration is that the same external fiber ring cavity could be used for self-injection locking of a DFB laser and as Brillouin scattering media to generate Stokes shifted optical wave [9,16]. However, a continuous laser operation at two frequencies has not been reported yet preventing it from many prosperous photonic applications.

It is worth noting that the fiber ring cavity is commonly used to generate highly coherent Brillouin wave from an external laser diode [24–26]. This method allows for a Stokes signal linewidth (< 1kHz) that is >10000 times narrower than the linewidth (~35 MHz) achievable through the traditional Brillouin scattering process in a long fiber. However, coupling between the DFB laser and a high-Q ring fiber cavity remains to be a technically complicated and cost consuming task [27,28]. In this paper, we introduce a simple dual-frequency laser configuration. In our approach, the implementation of self-injection locking into the Brillouin ring fiber laser helps to maintain coupling between the DFB laser and an external high-Q fiber cavity enabling dual-frequency laser operation. Specifically, the same ring fiber cavity is used to generate narrow-band light at the pump frequency (through self-injection locking mechanism) and narrow-band laser light at Stokes frequency (through stimulated Brillouin scattering). The system is supplied by a low-bandwidth active optoelectronic feedback circuit controlled by a low-cost USB-DAQ card that helps the laser to maintain the desired operation mode. We have explored key features of the laser performance, revealing its stability and applicability to RF harmonic generation of high spectral purity as an additional benefit of the proposed technique.

2. Experimental results and discussion

The principle of the laser operation in self-injection locking regime is explained in [19]. The radiation emitted by a DFB laser is passed through a high-Q ring cavity operating as a narrow-band pass filter (only the ring cavity mode frequency ν_R is passed) and injected back into the DFB laser cavity forcing the DFB laser to operate the frequency ν_R.

The experimental laser configuration is shown in Fig. 1(a). The semiconductor laser we use is a commercial distributed feedback (DFB) laser diode (MITSUBISHI FU-68PDF-V520M27B) assembled within a standard 14-pin butterfly package that is coupled to the fiber ring cavity through a circulator. The DFB laser delivering ~15 mW at ~1535.6 nm is equipped with a built-in optical isolator attenuating the power of backward radiation by $\kappa \sim 30\ dB$. The isolation κ is an important parameter of the laser model [19]. To support injection locking it should be between -25 and $-35\ dB$ that is a typical isolation of single stage optical fiber isolators. Such isolation is strong enough to prevent parasitic reflections, but too weak to eliminate the effect of optical feedback on DFB laser behavior.

The high-Q external ring cavity is spliced from two couplers (99/1) and (99/1). In order to implement the self-injection locking mechanism, the coupler redirects a part of the light circulating inside the cavity clockwise (CW) through the circulator (OC) back into the DFB laser thus providing passive feedback to the laser operation. The fiber configuration is spliced
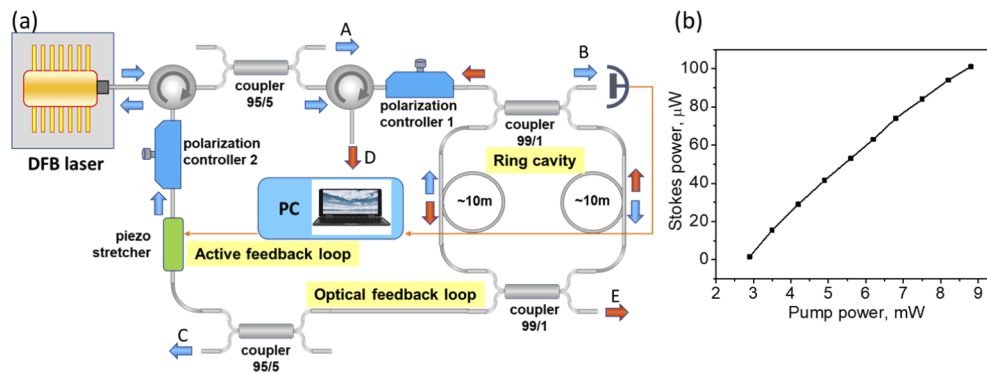
Fig. 1. (a) The experimental laser configuration; (b) Brillouin output power (port D) as a function of the DFB laser power at the fiber ring input.

from standard telecom components and placed into a foam box to reduce the influence of the laboratory environment. No additional thermal control of the box is applied.

Comparing the reported laser configuration [21] two crucial modifications have been implemented to achieve continuous dual-frequency lasing. The first modification concerns the operation of active feedback circuit. In order to explain the mechanism of laser stabilization, we have to adopt a very simplified view on the laser operation in self-injection locking regime. The detailed theoretical description of the laser operation is under progress and out of scope of this paper. The laser configuration shown in Fig. 1 could be thought as the high-Q ring cavity coupled with the second closed optical circuit (comprising the DFB laser cavity, upper fiber pass, half of the cavity ring and feedback loop fiber). The high-Q ring cavity sets the laser operation frequency ν_L to be one of the ring cavity mode frequencies ν_R. To make the laser operating self-injection locking $\nu_L = \nu_R$, the light at the frequency ν_R has to be also resonant in the second circuit, i.e. $\nu_R = \nu_{FB+LD}$, where ν_{FB+LD} is one of the second circuit eigen frequencies. Assuming the DFB laser cavity unchangeable (the laser diode current and temperature are well stabilized, the lasing power does not change), the environmental temperature variations affect the ring cavity and feedback loop fiber lengths changing the mutual position of the resonant frequencies ν_R and ν_{FB+LD}. A deviation of ν_R from ν_{FB+LD} (or versa) disrupts the injection locking regime causing mode-hopping. To avoid this, the position of ν_{FB+LD} should be permanently adjusted to ν_R maintaining the equality $\nu_{FB+LD} = \nu_R$. It is the task assigned to the active feedback loop. In [21] the active feedback has been implemented through the control of laser diode current. However, this solution is limited in its applications by rather a small range of allowed current modulation. Along with the useful effect on the DFB laser cavity refractive index connected with ν_{FB+LD}, a modulation of current could disturb many DFB laser parameters (power, temperature, gain) producing poorly predictable effects in the laser behavior. In contrast, the mechanism employed in this work (a piezo-activator attached to the feedback loop fiber) provides a direct tuning of ν_{FB+LD} just affecting the length of the feedback loop fiber as shown in Fig. 1(a). The piezo-activator is driven by a low-cost USB Multifunction DAQ (National Instrument NI USB-6009) connected to a PC. The laser power detected at port B serves as an error signal. The DAQ manages to keep it as low as possible adjusting the DAQ output voltage applied to the piezo-activator affecting the length of the optical fiber loop. By adjusting the DAQ output voltage (0 - 5 V), the piezo-stretcher maintains a continuous laser operation in self-injection locking regime keeping the matching between the feedback loop length and the ring cavity resonance that in its turn slowly drifts due to environmental temperature. We have found the new control mechanism to be more practical, exhibiting much better stability and reproducibility. In particular, it significantly expands the range of the laser frequency drifts acceptable for continuous laser operation in the self-injection

locking regime (>3 *GHz* in contrast to maximal ~1 *GHz* reported in [21]). The use of current control for the same purpose is found to be more limited and less predictable. In particular, at low output powers the laser operation becomes more sensitive to current modulation, i.e. even a low modulation of current might provoke mode-hopping events.

The second modification relates to a choice of the ring cavity length L_R. Specifically, we generate Brillouin lasing with the same fiber ring cavity that is already used for self-injection locking. Inside the ring the DFB laser radiation at v_L propagating CW is used to pump a Brillouin wave at $v_S = v_L - \Delta_{SBS}$ generating CCW, where Δ_{SBS} is the Brillouin frequency shift. Comparing our previous laser configuration [21] the ring fiber length L_R has been increased in 5 times (up to ~20 *m*) to decrease the Brillouin threshold. Besides, the ring cavity length has been precisely adjusted with the single-cut technique [29] to get perfect matching between the Brillouin frequency shift Δv_{SBS} and the ring cavity free spectrum range $FSR \equiv c/nL_R$ (FSR), where c is the speed of light and n is the fiber refractive index. So that $\Delta v_{SBS} = m_B FSR$, where m_B is an integer. With the perfectly adjusted fiber ring cavity active stabilization of lasing at $v_L = v_R$ ensures stabilization of lasing at the frequency v_S.

For the dual-frequency laser configuration shown in Fig. 1(a), lasing at the pump frequency v_L could be monitored through the ports A, B, C and at the Brillouin frequency v_S through the ports D, E. The ports A and D are used as the main laser outputs. The reflected signal from the port B is detected by a fast photodetector and is used as an error signal for the active feedback operation. The ports C and E are used as control points for laser characterization. While the DFB laser operates in a free-running regime, its linewidth is estimated to be ~10 MHz, the most of the DFB laser power is reflected by the ring cavity and released through the port B. The power recorded at the port C is negligible (the detectable level is ~60 *nW* at ~1 *mW* of port B power). Self-injection-locking causes drastic narrowing of the laser linewidth down to kHz range leading to a decrease of the power released through the port B and an increase of the power emitted through the port C. So, monitoring the reflected power through the ports B (the error signal) allows evaluating the efficiency of the laser linewidth narrowing due to self-injection locking and helps to maintain a continuous laser operation in the self-injection-locking regime avoiding mode-hopping. This task is assigned to the optoelectronic feedback circuit. When CW power inside the ring cavity exceeds the Brillouin lasing threshold, the CCW wave is emitted through the port D.

Figure 1(b) shows the experimental dependence of the laser power at the Stokes frequency v_S detected in port D on the laser power at the pump frequency v_L detected in port A. No power conversion to the Stokes frequency is detected below the pump power threshold of ~2.9 mW. Above the threshold the efficiency of pump-to-Stokes frequency conversion is estimated to be ~3.3% that is good enough for many potential laser applications (e.g. Brillouin sensing).

Figure 2 compares the laser operation with and without active feedback. Typical oscilloscope traces recorded with the reflected, transmitted and Brillouin powers (ports B, C, and D, respectively) without active feedback are shown in Fig. 2(a). Most of the time the reflected and transmitted powers (ports B and C, respectively) change synchronously in anti-phase. The observed behavior can be interpreted in terms of the laser frequency deviation from the ring cavity resonance $\delta v_{LR} = v_L - v_R$. It is an inherent property of the ring cavity: the higher deviation $|\delta v_{LR}|$ the higher reflected power P_B detected at the port B and the lower transmitted power detected at the port C. Driven by an environment noise the ring resonance frequency v_R slowly varies in time forcing the reflected power P_B to walk between its minimal and maximal values. When approaching its minimum value, the recorded reflected power P_B keeps it for a while highlighting the laser operation in the self-injection locking regime ($\delta v_{LR} = 0$). In this regime the length of feedback loop fiber perfectly matches the ring cavity resonance, i.e. $v_{FB+LD} = v_R$ and the laser works against the temperature fluctuations to maintain $\delta v_{LR} \to 0$ [19]. An increase of the laser power circulating CW inside the ring above the Brillouin lasing threshold causes lasing of the

contra-propagating Brillouin CCW wave at ν_S detected at the port D. Energy conversion from the pump to the Stokes wave maintains the transmitted laser power detected at the port C at the level corresponding to the Brillouin threshold. Further temperature drift of the ring resonance frequency ν_R violates the equality $\nu_R = \nu_{FB+LD}$ pulling the laser to generate frequency ν_L different from ν_R thus causing an increase of $|\delta\nu_{LR}|$. This increase is followed by an increase of the reflected power P_B and decrease of the CW pump power at ν_L circulating inside the ring. When the pump power inside the ring falls below the Brillouin threshold, lasing at the Stokes frequency disrupts. With stronger violation of the equality $\nu_R = \nu_{FB+LD}$, $|\delta\nu_{LR}|$ increases further and the reflected power P_B approaches its maximal value, where mode-hopping to the different ring cavity mode occurs disturbing the laser stability and impairing the laser performance characteristics.
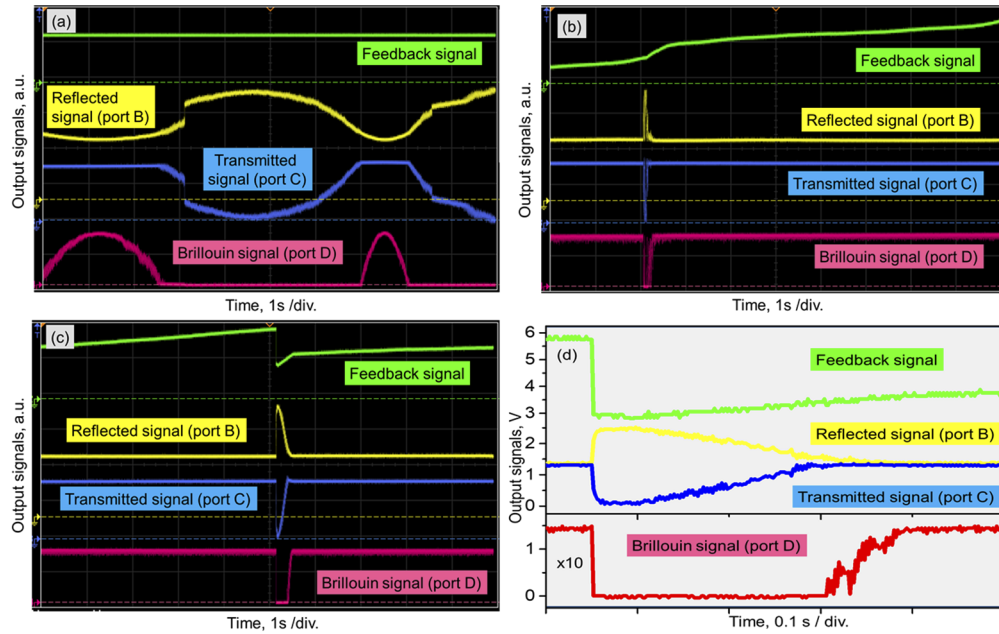

Fig. 2. Typical oscilloscope traces of reflected (yellow curves), transmitted (blue curves) and Brillouin (red curve) optical power and active feedback control signal (green curve); (a) the laser operation with optical feedback only; (b) optical and electronic feedbacks - responses on knock on the fiber ring; (c) optical and electronic feedbacks - responses on a jump of the feedback control signal; (d) a zoom of oscilloscope traces (c). The dashed lines mark zero levels.

The laser operation with active feedback is shown in Figs. 2(b) and 2(c). The optoelectronic feedback circuit is trying to maintain the reflected power P_B detected at the port B (now it is used as an error signal) fixed to its minimal value. So, the DFB laser frequency ν_L is always locked to the ring cavity mode ν_R providing a stable laser operation at the pump and Brillouin frequencies recorded at ports A and D, respectively ($\nu_L = \nu_R = \nu_{FB+LD}$). One can see that the self-injection locking mechanism in combination with optoelectronic feedback perfectly works against the environment noise enabling stable laser operation at two locked frequencies. All optical power traces are almost flat and exhibits no fluctuations.

A few experiments have been performed for characterizing the laser operation in the stabilized regime. First, we have determined time constants associated with the feedback mechanism. Figure 2(b) presents the system response to a short pencil kick on the fiber configuration. When the configuration is perturbed, it exhibits a variety of dynamical behaviors [24]. Clearly, the system behaves as a high-pass filter, since high frequency acoustic perturbations cannot be

compensated by the slow acting feedback. Following these perturbations, the error signal P_B (and so the laser frequency) makes a number of stochastic fluctuations until recoils and returns to the original point in an exponential decay manner. The typical time constant of the feedback mechanism is $\tau_L \sim 0.2\ s$. Brillouin lasing is more sensitive, it disrupts almost immediately after a kick and starts to restore only after the complete restoration of the pump lasing. A typical time constant of Stokes power restoration is much shorter $\tau_S \sim 0.05\ s$.

Figures 2(c) and 2(d) shows a system response on a jump of the active feedback control signal forcing the laser configuration to switch the current pump frequency (see the feedback signal trace). One can see that, in this case, the pump laser accepts the frequency change providing exponential relaxation to new state with the same time constant of $\tau_L \sim 0.2\ s$. Note that Brillouin lasing disrupts immediately after the current jump and starts to restore with the time constant of $\tau_S \sim 0.05\ s$ just after the pump laser frequency transition is completed. These specific features are in a good agreement with the predictions of the self-injection locking and Brillouin lasing models [19,26].

To evaluate polarization properties of the dual-frequency laser, the light emitted from the pump and Stokes laser outputs (port A and D, respectively) has been tested by a polarization analyzer (HP 8509A\B). The results obtained for the laser operating without and with active feedback are shown in Fig. 3. The Stokes parameters are related to the polarization attractor at the Poincaré sphere in the form of a fixed point measured for a few observed laser regimes. When the degree of polarization (DOP) is close to 100%, the fixed point at the Poincaré sphere indicates a stable operation. For the laser operation without active feedback the pump wave attractor makes a precession with a small radius around a single point [Fig. 3(a)], its DOP is estimated to be ~98%. The polarization dynamics of the Stokes wave (when it is generated) takes the form of unpredictable wandering [Fig. 3(d)]. In contrast, for the laser operation with active feedback, attractors for both laser outputs are fixed points at the Poincaré sphere, i.e. there DOP are close to 100% [Figs. 3(c), 3(f)]. Figures 3(b) and 3(e) presents the polarization dynamics of laser making transition to new pump frequency after a jump of active feedback control signal [see, Figs. 2(c), 2(d)]. The pump wave attractor exhibits behavior [Fig. 3(b)] similar to that of laser without active feedback [Fig. 3(a)]. It makes a precession around a single point with a small
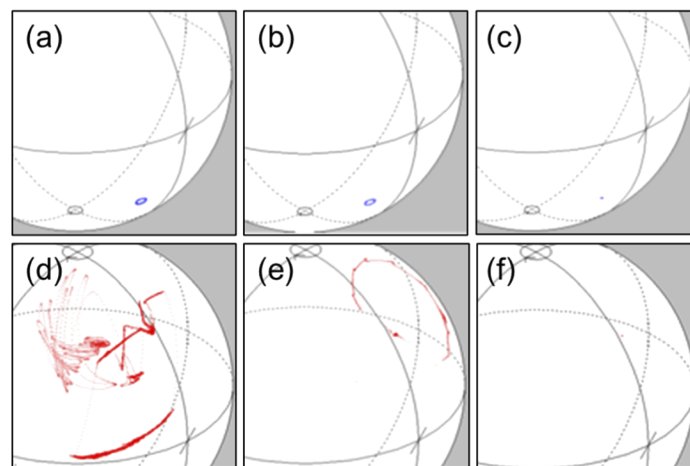

Fig. 3. Typical state of polarization (SOP) trajectories on Poincare sphere for the reflected pump (port B, a-c) and Brillouin (port D, d-f) signals. (a, d) laser operation with optical feedback only; (b, e) optical and electronic feedbacks - responses on a jump of active feedback control signal; (c, f) optical and electronic feedbacks without perturbations.

radius, its DOP is estimated to be ~97% and the polarization state does not change in spite of the change of pump frequency. The Stokes wave attractor makes a precession with much larger radius approaching the final point that could differ from the starting point [Fig. 3(e)], its DOP is estimated to be ~60%. Note that the DOP of the pump radiation measured in the port A does not depends on the DFB laser operation mode and is always close to ~100%.

A delayed self-heterodyne technique has been employed to measure the linewidths of laser radiation emitted through two laser outputs [30–35]. An all-fiber unbalanced Mach–Zehnder interferometer with a 55 km delay fiber and 25 MHz phase modulator supplied by a polarization controller is used for this purpose. The beat signal from the interferometer is detected by a ~5 GHz photodiode and analyzed by an RF spectrum analyzer (FSH8, Rohde & Schwarz). The experimental spectra shown in Fig. 4 are averaged over 10 realizations each. Both spectra are centered around 25 *MHz*. The narrower spectrum (recorded with the Stokes output) exhibits oscillations in the wings evidencing that the laser coherence length is much longer than the interferometer delay fiber [31].
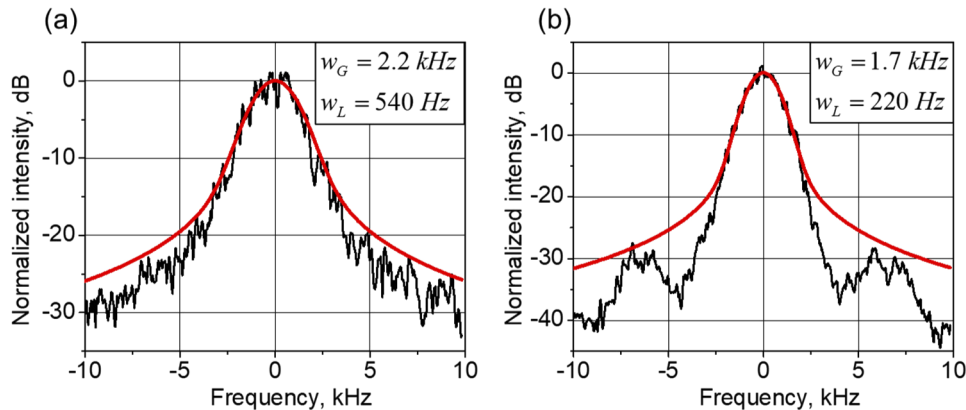

Fig. 4. Delayed self-heterodyne spectra of the laser radiation emitted through ports A (a) and D (b) at pump and Stokes laser frequencies, respectively. The measured spectra (black) and their fitting Voigt profiles (red) with the Gaussian and Lorentzian linewidths (FWHM) w_G and w_L, respectively, as the fitting parameters.

To proceed the measured data, we use the method based on the decomposition of the self-heterodyne spectra into Gaussian and Lorentzian contributions [32,34]. In this approach, the laser's line is thought to be Gaussian in the range near the top, and Lorentzian in the wings. Long delay fiber results in considerable broadening of the self-heterodyne spectrum due to the $1/f$ frequency noise. The convolution with the acquired $1/f$ noise causes overestimation of the natural laser linewidth, if it is estimated from the 3-dB width of self-heterodyne spectrum as commonly used [30]. Since, the $1/f$ noise contributes Gaussian broadening mostly pronounced near the top of the laser spectrum, the estimation by the 20-dB width of self-heterodyne spectrum is closer to the natural laser linewidth, however, the result is still overestimating [32]. The measured self-heterodyne spectrum is actually the Voigt profile, i.e., the convolution of the Lorentzian and Gaussian spectra. The Lorentzian and Gaussian contributions can be evaluated by fitting the measured self-heterodyne spectrum by the Voigt profile. Figure 4 shows the fitting Voigt profiles obtained using the algorithm described in [34]. One can see that the fitting is applied just to the highest points in the wings ensuring upper values of the Lorentzian laser linewidths estimated for two laser outputs. The Lorentzian laser linewidth is a half of the Lorentzian width (FWHM) w_L of self-heterodyne spectrum and the Gaussian component is $\sqrt{2}/2$ times the Gaussian linewidth (FWHM) w_G of self-heterodyne spectrum [32]. Therefore, the natural

Lorentzian laser linewidths are found to be narrower than 270 Hz and 110 Hz for the pump and Stokes laser outputs, respectively. These results are in a good agreement with the direct measurements of the radio-frequency (RF) spectrum characterizing the beating between pump and Stokes laser outputs demonstrated below.

Noise performance of the dual-frequency laser configuration is presented in Fig. 5. Figure 5(a) depicts the power spectral density (PSD) of phase noise measured for the pump, Stokes, transmitted and reflected radiations with a RF spectrum analyzer (Agilent N9320A) in the range of $10 - 100$ *kHz*. For this RF range the effect of active feedback noise on the laser performance is negligible. The PSDs have been measured by the self-heterodyne method [36–38] using an unbalanced Mach–Zehnder interferometer with a ~1.3 *km* delay fiber (~5.76 *µs*) and 20 *MHz* frequency shifter. One can see that the used active stabilization minimizes the phase noise in all laser ports. In particular, comparing with free-running laser the PSD measured with pump laser output (port A) is lower by ~$(35 - 40)$ *dBc/Hz*. Comparing the pump laser output (port A) the PSD measured with Brillouin laser output (port D) is lower by ~$(7 - 15)$ *dBc/Hz*. Note, the pump radiation passed through the ring (transmitted and reflected) exhibits the PSD that is lower by ~$(3 - 10)$ *dBc/Hz* than the PSD measured with the direct pump laser output (port A). We believe that it is the result of filtering effect in the ring cavity.
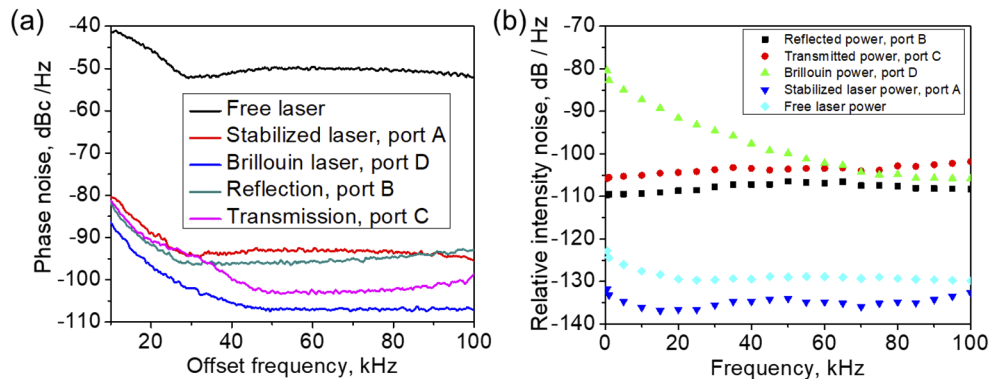

Fig. 5. Noise performance of the laser. a) Phase noise; b) Relative Intensity noise (RIN).

Figure 5(b) presents the relative intensity noise (RIN) measured with a lock-in amplifier SRS510 in $1 - 100$ *kHz* frequency interval. One can see that the RIN of stabilized pump laser is lower by ~$(5 - 10)$ *dB* than the RIN of free-running DFB laser. At the same time, the RIN of the Stokes radiation (port D) is higher by $30 - 40$ *dB* then the RIN of the pump laser output (port A), especially at lower frequencies. We explain this increase by an exponential manner of the Stokes wave amplification in the fiber ring cavity resulting in a strong pump-to-Stokes RIN transfer. One can see, that the additional RIN induced by the Brillouin lasing in the cavity is also transferred to the reflected and transmitted pump RINs causing their increase by $30 - 40$ *dB* in comparison with the pump laser radiation.

Finally, the radiofrequency (RF) spectrum characterizing the beating between pump and Stokes laser outputs (A and D, respectively) mixed in a single fiber has been evaluated with RF signal analyzer (Keysight N9040B, 50GHz). Figure 6(a) presents a typical spectrum recorded with an acquisition time of ~20 *ms*. The spectrum exhibits a pronounced peak with the center at ~10946.3098 *MHz* and the width of ~290 *Hz*. The peak frequency corresponds to the Brillouin frequency shift in the ring cavity fiber (SMF-28, Corning Inc.) at 1535 nm. The peak width is in a good agreement with the Lorentz linewidths estimated for the pump and Stokes laser outputs with the self-heterodyne technique (see Fig. 4). Acquiring the RF spectrum with longer times leads to remarkable broadening of the spectrum due to drift of the spectrum position caused

by environmental noise. Figure 6(b) demonstrates a typical spectrum acquired for ~5 min. It exhibits a width of ~1800 Hz that is 6 times the width of the instantaneously measured spectrum shown in Fig. 6(a).
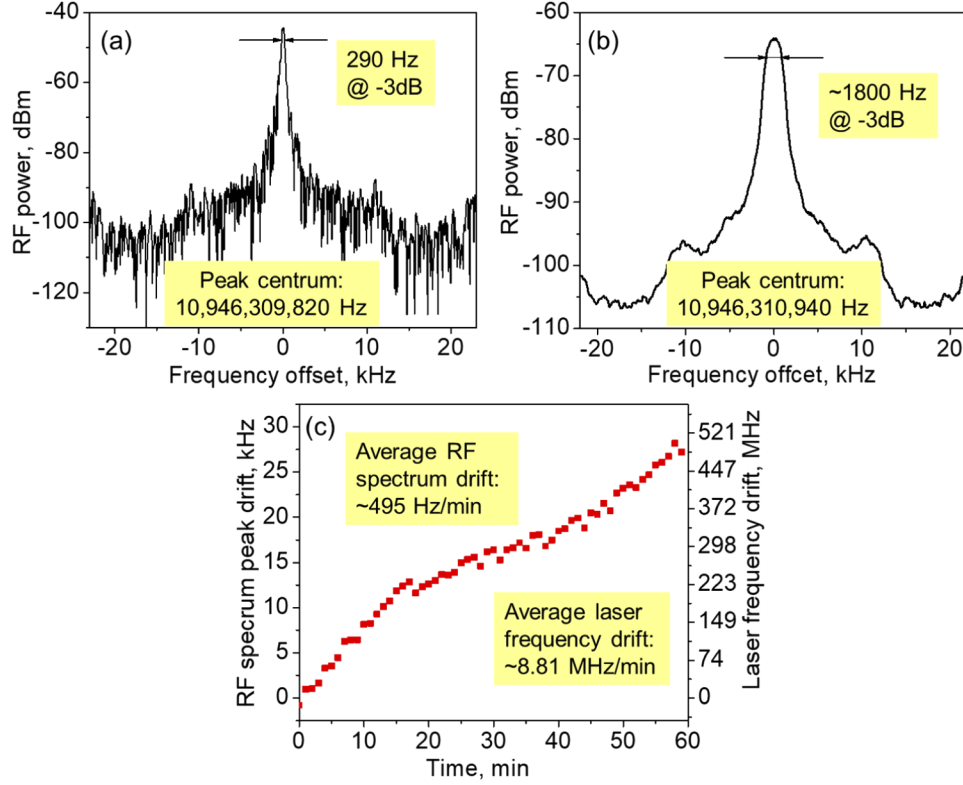

Fig. 6. RF beat spectrum evolution. (a) RF beat spectrum acquired for ~20 ms; (b) RF beat spectrum averaged for 5 min; (c) evolution of the RF beat spectrum peak frequency measured each minute for 60 minutes.

Due to the effect of environmental noise on the laser configuration, the pump and Stokes laser frequencies emitted through the port A and D, respectively, slowly vary in time. These frequency variations are referred to as a long-term laser frequency drift [20]. For the continuous laser operation in self-injection locking regime, the DFB laser frequency is strongly locked to the ring cavity resonance $\nu_R = mc/nL_R$, where m is an integer number. Therefore, the long-term laser frequency drift is mainly determined by a change of the ring cavity optical length $\delta(nL_R)$ caused by the environmental temperature variations. The laser operation in dual frequency mode allows to monitor the laser frequency drift by recording the peak frequency of RF beat spectrum similar to that shown in Fig. 6(a). Indeed, the generated laser frequencies ν_L (pump, port A) and ν_S (Stokes, port D) are both the resonant ring cavity modes, i.e. $\nu_{L,S} = m_{L,S}c/nL_R$, where $m_{L,S}$ are integer numbers. Therefore, their drifts $\delta\nu_L(t) = \nu_L(t) - \nu_L(0)$ and $\delta\nu_S(t) = \nu_S(t) - \nu_S(0)$ for time t are strongly linked to the change of the ring cavity optical length $\delta(nL_R)$ acquired for the same time. The measured drift of the RF spectrum peak frequency $\delta\nu_B = \delta\nu_L - \delta\nu_S$ is determined by the drifts of the laser frequencies $\delta\nu_L$ and $\delta\nu_S$, and, therefore, all of them are linked to $\delta(nL_R)$ as:

$$\frac{\delta\nu_L}{\nu_L} = \frac{\delta\nu_S}{\nu_S} = \frac{\delta\nu_B}{\nu_B} = -\frac{\delta(nL_R)}{nL_R}. \tag{1}$$

From Eq. (1) the laser long-term frequency drift $\delta\nu_L = \delta\nu_B(\nu_L/\nu_B)$ is directly expressed through $\delta\nu_B$ making possible its long-term monitoring by permanent measurements of the RF spectrum peak frequency. A typical evolution of the RF spectrum peak frequency recorded for 1h (one per minute) is shown in Fig. 6(c). One can see, it increases monotonically with a typical rate of ~0.5 kHz/min passing a range of ~30 kHz. The same data describes the drift of the laser frequency. It occurs within the range of ~520MHz and has a typical rate of ~8.8MHz/min that is in a good agreement with the value reported earlier under similar conditions (~10MHz/min) [18,20]. Note that the spliced laser configuration is placed into a foam box to reduce the influence of the laboratory environment. No additional thermal control or any particular vibration and acoustics insulation protections are used.

3. Conclusion

In conclusion, we have introduced a simple dual-frequency laser based on a DFB laser coupled to an all-fiber ring cavity and working in self-injection-locking regime. In our laser configuration, the same ring fiber cavity is exploited both for self-injection locking of the DFB laser and for generation of Stokes light via stimulated Brillouin scattering. A low-cost USB-DAQ is used to stabilize the system preventing mode-hopping. Importantly, a stable laser operation at two mutually locked frequencies is provided by the self-injection locking mechanism, while the active feedback loop just helps the laser to operate in this regime. Besides, the self-injection locking mechanism maintains permanent coupling between the DFB laser and the external fiber ring cavity enabling perfect resonant pumping for low-noise Brillouin lasing.

The dual-frequency laser performance is quite impressive considering that no significant attempt has been made to temperature stabilize the set-up. The laser output powers are ~9 mW and ~100 μW for pump and Stokes outputs, respectively. Further power scaling is still possible with external amplifiers. The pump laser power could be amplified with an Erbium-doped fiber amplifier (EDFA), while the use of an external Brillouin amplifier (built from the same fiber as the ring cavity and pumped by the laser power amplified in EDFA) is preferable for narrow-band Stokes beam amplification. The laser operation frequencies are strongly locked to the ring cavity resonances and their drift measured in the experiment (~8.8 MHz/min) is mainly determined by environmental temperature variations. The use of an additional thermal control applied to the whole laser configuration and supported by permanent monitoring of the RF spectrum peak frequency (similar to that shown in Fig. 6(a) could further reduce the laser frequency drift and minimize long-term RF spectral broadening. The limiting factor here is the mechanical piezo-actuator generating an acoustic noise in the feedback fiber loop. The use of a phase modulator instead of the piezo-actuator could eliminate the acoustic noise minimizing the laser frequency drift. The use of polarization maintaining (PM) fiber configuration allows to omit polarization controllers. However, PM fiber components commonly possess higher linear losses that are crucial for high-Q fiber cavities.

In general, the reported results improve our understanding of the self-injection-locking mechanism in semiconductor lasers and open up new possibilities for manipulating and controlling their properties. In this work, we have finally identified the main reason for laser instabilities (periodic interruption of the laser operation accompanied by mode-hopping events) observed in earlier works [9,15,16]. It is violation of the equality $\nu_R = \nu_{FB+LD}$ in the laser configuration caused by environmental temperature variations. New ability to generate continuously two locked frequencies is attractive for many laser applications, including high-resolution spectroscopy, phase coherent optical communications, distributed fiber optics sensing, coherent optical spectrum analyzer, and microwave photonics. In particular, the reported laser characteristics are well superior to the requirements to the laser modules commonly used with Brillouin Optical Time Domain Analyzer (BOTDA). In nearest future, translating the proposed laser design to integrated

photonics [39–46] will dramatically reduce cost and footprint for many applications such as ultra-high capacity fiber and data center networks, atomic clocks, and microwave photonics.

Funding

Acknowledgments

Disclosures

The authors declare no conflicts of interest.

References

1. B. Stern, X. Ji, A. Dutt, and M. Lipson, "Compact narrow-linewidth integrated laser based on a low-loss silicon nitride ring resonator," Opt. Lett. **42**(21), 4541–4544 (2017).
2. R. Legaie, C. J. Picken, and J. D. Pritchard, "Sub-kilohertz excitation lasers for quantum information processing with rydberg atoms," J. Opt. Soc. Am. B **35**(4), 892–898 (2018).
3. T. Komljenovic, M. Davenport, J. Hulme, A. Y. Liu, C. T. Santis, A. Spott, S. Srinivasan, E. J. Stanton, C. Zhang, and J. E. Bowers, "Heterogeneous silicon photonic integrated circuits," J. Lightwave Technol. **34**(1), 20–35 (2016).
4. D. Leandro, V. deMiguel-Soto, and M. López-Amo, "High-resolution sensor system using a random distributed feedback fiber laser," J. Lightwave Technol. **34**(19), 4596–4602 (2016).
5. J. L. Bueno Escobedo, V. V. Spirin, C. A. López-Mercado, A. Márquez Lucero, P. Mégret, I. O. Zolotovskii, and A. A. Fotiadi, "Self-injection locking of the dfb laser through an external ring fiber cavity: Application for phase sensitive otdr acoustic sensor," Results Phys. **7**, 641–643 (2017).
6. D. K. Shin, B. M. Henson, R. I. Khakimov, J. A. Ross, C. J. Dedman, S. S. Hodgman, K. G. Baldwin, and A. G. Truscott, "Widely tunable, narrow linewidth external-cavity gain chip laser for spectroscopy between 1.0–1.1 μm," Opt. Express **24**(24), 27403–27414 (2016).
7. Z. Fang, H. Cai, G. Chen, and R. Qu, *Single frequency semiconductor lasers* (Springer, 2017).
8. H. Guan, A. Novack, T. Galfsky, Y. Ma, S. Fathololoumi, A. Horth, T. N. Huynh, J. Roman, R. Shi, and M. Caverley, "Widely-tunable, narrow-linewidth iii-v/silicon hybrid external-cavity laser for coherent communication," Opt. Express **26**(7), 7920–7933 (2018).
9. V. V. Spirin, C. A. López-Mercado, P. Mégret, and A. A. Fotiadi, "Single-mode brillouin fiber laser passively stabilized at resonance frequency with self-injection locked pump laser," Laser Phys. Lett. **9**(5), 377–380 (2012).
10. K. Petermann, *Laser diode modulation and noise* (Springer Science & Business Media, 2012).
11. J. Ohtsubo, *Semiconductor lasers: Stability, instability and chaos* (Springer, 2012).
12. R. Galiev, N. Pavlov, N. Kondratiev, S. Koptyaev, V. Lobanov, A. Voloshin, A. Gorodnitskiy, and M. Gorodetsky, "Spectrum collapse, narrow linewidth, and bogatov effect in diode lasers locked to high-q optical microresonators," Opt. Express **26**(23), 30509–30522 (2018).
13. W. Liang, V. Ilchenko, D. Eliyahu, A. Savchenkov, A. Matsko, D. Seidel, and L. Maleki, "Ultralow noise miniature external cavity semiconductor laser," Nat. Commun. **6**(1), 7371–73766 (2015).
14. S. Huang, T. Zhu, G. Yin, T. Lan, F. Li, L. Huang, and M. Liu, "Dual-cavity feedback assisted dfb narrow linewidth laser," Sci. Rep. **7**(1), 1185 (2017).
15. C. A. López-Mercado, V. V. Spirin, J. L. Bueno Escobedo, A. Márquez Lucero, P. Mégret, I. O. Zolotovskii, and A. A. Fotiadi, "Locking of the dfb laser through fiber optic resonator on different coupling regimes," Opt. Commun. **359**, 195–199 (2016).
16. V. V. Spirin, C. A. López-Mercado, D. Kinet, P. Mégret, I. O. Zolotovskiy, and A. A. Fotiadi, "A single-longitudinal-mode brillouin fiber laser passively stabilized at the pump resonance frequency with a dynamic population inversion grating," Laser Phys. Lett. **10**(1), 015102 (2013).
17. J. L. Bueno Escobedo, V. V. Spirin, C. A. López-Mercado, P. Mégret, I. O. Zolotovskii, and A. A. Fotiadi, "Self-injection locking of the dfb laser through an external ring fiber cavity: Polarization behavior," Results Phys. **6**, 59–60 (2016).
18. J. L. Bueno Escobedo, J. Jason, C. A. López-Mercado, V. V. Spirin, M. Wuilpart, P. Mégret, D. A. Korobko, I. O. Zolotovskiy, and A. A. Fotiadi, "Distributed measurements of vibration frequency using phase-otdr with a dfb laser self-stabilized through pm fiber ring cavity," Results Phys. **12**, 1840–1842 (2019).
19. D. A. Korobko, I. O. Zolotovskii, K. Panajotov, V. V. Spirin, and A. A. Fotiadi, "Self-injection-locking linewidth narrowing in a semiconductor laser coupled to an external fiber-optic ring resonator," Opt. Commun. **405**, 253–258 (2017).

20. F. Wei, F. Yang, X. Zhang, D. Xu, M. Ding, L. Zhang, D. Chen, H. Cai, Z. Fang, and G. Xijia, "Subkilohertz linewidth reduction of a dfb diode laser using self-injection locking with a fiber bragg grating fabry-perot cavity," Opt. Express **24**(15), 17406–17415 (2016).
21. V. V. Spirin, J. L. Bueno Escobedo, D. A. Korobko, P. Mégret, and A. A. Fotiadi, "Stabilizing dfb laser injection-locked to an external fiber-optic ring resonator," Opt. Express **28**(1), 478–484 (2020).
22. T. Hansch and B. Couillaud, "Laser frequency stabilization by polarization spectroscopy of a reflecting reference cavity," Opt. Commun. **35**(3), 441–444 (1980).
23. J. Alnis, A. Matveev, N. Kolachevsky, T. Udem, and T. Hänsch, "Subhertz linewidth diode lasers by stabilization to vibrationally and thermally compensated ultralow-expansion glass fabry-pérot cavities," Phys. Rev. A **77**(5), 053809 (2008).
24. O. Kotlicki and J. Scheuer, "Thermal self-stability, multi-stability, and memory effects in single-mode brillouin fiber lasers," Opt. Express **25**(22), 27321–27333 (2017).
25. D. Korobko, I. Zolotovskii, V. Svetukhin, A. Zhukov, A. Fomin, C. Borisova, and A. Fotiadi, "Detuning effects in brillouin ring microresonator laser," Opt. Express **28**(4), 4962–4972 (2020).
26. C. E. Preda, A. A. Fotiadi, and P. Megret, "Numerical approximation for brillouin fiber ring resonator," Opt. Express **20**(5), 5783–5788 (2012).
27. L. Rossi, D. Marini, F. Bastianini, and G. Bolognini, "Analysis of enhanced-performance fibre brillouin ring laser for brillouin sensing applications," Opt. Express **27**(20), 29448–29459 (2019).
28. M. V. G. Danion, L. Frein, P. Szriftgiser, and M. Alouini, "Brillouin assisted optoelectronic self-narrowing of laser linewidth," IEEE Photonics Technol. Lett. **31**(12), 975–978 (2019).
29. V. V. Spirin, C. A. López-Mercado, S. I. Kablukov, E. A. Zlobina, I. O. Zolotovskiy, P. Mégret, and A. A. Fotiadi, "Single cut technique for adjustment of doubly resonant brillouin laser cavities," Opt. Lett. **38**(14), 2528–2531 (2013).
30. D. Derickson, C. Hentschel, and J. Vobis, *Fiber optic test and measurement* (Prentice Hall PTR New Jersey, 1998).
31. L. E. Richter, H. I. Mandelberg, M. S. Kruger, and P. A. Mcgrath, "Linewidth determination from self-heterodyne measurements with subcoherence delay times," IEEE J. Quantum Electron. **22**(11), 2070–2074 (1986).
32. L. B. Mercer, "1 /f frequency noise effects on self-heterodyne linewidth measurements," J. Lightwave Technol. **9**(4), 485–493 (1991).
33. P. Horak and W. H. Loh, "On the delayed self-heterodyne interferometric technique for determining the linewidth of fiber lasers," Opt. Express **14**(9), 3923–3928 (2006).
34. M. Chen, Z. Meng, J. Wang, and W. Chen, "Ultra-narrow linewidth measurement based on voigt profile fitting," Opt. Express **23**(5), 6803–6808 (2015).
35. G. Di Domenico, S. Schilt, and P. Thomann, "Simple approach to the relation between laser frequency noise and laser line shape," Appl. Opt. **49**(25), 4801–4807 (2010).
36. S. Camatel and V. Ferrero, "Narrow linewidth cw laser phase noise characterization methods for coherent transmission system applications," J. Lightwave Technol. **26**(17), 3048–3055 (2008).
37. O. Llopis, P. H. Merrer, H. Brahimi, K. Saleh, and P. Lacroix, "Phase noise measurement of a narrow linewidth cw laser using delay line approaches," Opt. Lett. **36**(14), 2713–2715 (2011).
38. Y. Li, Z. Fu, L. Zhu, J. Fang, H. Zhu, J. Zhong, P. Xu, X. Chen, J. Wang, and M. Zhan, "Laser frequency noise measurement using an envelope-ratio method based on a delayed self-heterodyne interferometer," Opt. Commun. **435**, 244–250 (2019).
39. B. J. Eggleton, C. G. Poulton, P. T. Rakich, M. J. Steel, and G. Bahl, "Brillouin integrated photonics," Nat. Photonics **13**(10), 664–677 (2019).
40. H. H. Diamandi and A. Zadok, "Ultra-narrowband integrated brillouin laser," Nat. Photonics **13**(1), 9–10 (2019).
41. S. Gundavarapu, G. M. Brodnik, M. Puckett, T. Huffman, D. Bose, R. Behunin, J. Wu, T. Qiu, C. Pinho, N. Chauhan, J. Nohava, P. T. Rakich, K. D. Nelson, M. Salit, and D. J. Blumenthal, "Sub-hertz fundamental linewidth photonic integrated brillouin laser," Nat. Photonics **13**(1), 60–67 (2019).
42. S. R. Mirnaziry, C. Wolff, M. J. Steel, B. J. Eggleton, and C. G. Poulton, "Stimulated brillouin scattering in integrated ring resonators," J. Opt. Soc. Am. B **34**(5), 937–949 (2017).
43. N. T. Otterstrom, R. O. Behunin, E. A. Kittlaus, Z. Wang, and P. T. Rakich, "A silicon brillouin laser," Science **360**(6393), 1113–1116 (2018).
44. B. Morrison, A. Casas-Bedoya, G. Ren, K. Vu, Y. Liu, A. Zarifi, T. G. Nguyen, D.-Y. Choi, D. Marpaung, and S. J. Madden, "Compact brillouin devices through hybrid integration on silicon," Optica **4**(8), 847–854 (2017).
45. D. Marpaung, J. Yao, and J. Capmany, "Integrated microwave photonics," Nat. Photonics **13**(2), 80–90 (2019).
46. J. Li, M.-G. Suh, and K. Vahala, "Microresonator brillouin gyroscope," Optica **4**(3), 346–348 (2017).